Complex atomic spectral line shapes in the presence of an external magnetic field

M. L. Adams*
Department of Nuclear Engineering, Massachusetts Institute of Technology, NW16-230, 167 Albany Street, Cambridge, Massachusetts 02139

R. W. Lee, H. A. Scott, and H. K. Chung
University of California, Lawrence Livermore National Laboratory, P.O. Box 808, Livermore, California 94551

L. Klein
Department of Physics and Astronomy, Howard University, Washington, DC 20059
(Received 2 August 2002; published 20 December 2002)

Both the theoretical basis and the computational approach for extending the capabilities of an established spectral line broadening code are presented. By following standard line broadening theory, the effects of an external magnetic field are incorporated into the plasma average and atomic Hamiltonian. An external magnetic field introduces a preferential axis that destroys the symmetry of the quasistatic electric ion microfield. An external magnetic field also modifies the angular properties of the atomic Hamiltonian—atomic energy levels are perturbed and the spectral emission line is polarized. These extensions have been incorporated in an atomic line shape code for complex atoms and applied to several problems of importance to the understanding of tokamak edge plasmas. Applications fall into two broad categories: (1) determination of local plasma properties, such as the magnetic field strength, from distinct line shape features; and (2) consideration of global plasma phenomenon, such as radiation transport. Observable features of the Zeeman effect make H_α a good line for diagnosing the magnetic field. H_β does not make a good electron density diagnostic since the Zeeman effect is comparable to the Stark effect for a majority of tokamak edge plasma conditions. For optically thick lines, the details of the spectral line shapes are shown to significantly influence the transport of radiation throughout the system.

DOI: 10.1103/PhysRevE.66.066413 PACS number(s): 52.70.−m, 32.70.−n, 52.55.Fa

I. INTRODUCTION

Plasma properties in the tokamak edge typically span several orders of magnitude at any given time during a typical experiment [1,2]. The system properties generally span the following range: $10^{12}<n_e(\mathrm{cm}^{-3})<10^{16}$, $0.1<T_e(\mathrm{eV})<500.0$, and $0.1<B(\mathrm{T})<10.0$; where n_e is the electron density, T_e is the electron temperature, and B is the magnetic field strength (with permeability set to unity). While this large variation in plasma conditions poses many important theoretical and computational challenges, for the present spectral line shape study the high-density low-temperature (HDLT) edge plasma regions are of particular interest [3].

The HDLT plasmas are found in detached divertor experiments near the divertor target plate and in Marfes (an axisymmetric radiating phenomenon that is poloidally localized in the plasma edge). In ALCATOR C-Mod, HDLT plasma properties are of the order: $n_e\sim10^{15}$ cm^{-3}, $T_e\sim1.0$ eV, $B\sim6$ T in a region of characteristic spatial extent $L\sim3$ cm. What makes these plasmas especially interesting is that they are partially ionized (there exists a significant fraction of neutral particles in the edge plasma) and they interact strongly with line radiation (optical depths are much greater than unity). Thus, in HDLT plasmas, the details of spectral line shapes will be important to the spatial and frequency variations of the radiation field, which in turn influences the spatial variation in level populations and ultimately the transport of (nonradiative) energy. It is this connection between the energy transport and the details of spectral line shapes that motivates this research.

Investigating radiation effects on plasma transport in tokamak edge plasmas requires a spectral line shape code that includes the effects of an external magnetic field and is numerically fast so that it can be integrated into larger transport codes. Since the source of radiation can come from hydrogenic and nonhydrogenic atoms, such as carbon and boron, we also seek to produce a spectral line shape code that applies to atoms with complex structure. These goals are accomplished by considering both the theoretical and computational aspects that pertain to incorporating magnetic effects into the many electron atom spectral line broadening model TOTAL [4]. The resulting model is named TOTALB.

To set the stage for the current paper, a brief history of magnetic line broadening is presented. The effect of an external magnetic field on spectral line shapes was initially studied by Hoe *et al.* [5], a decade after the seminal papers on pressure broadening by Baranger [6] and Kolb-Griem [7]. Drawin *et al.* [8] experimentally verified the theoretical work of Hoe *et al.* [5] by using a straight discharge tube surrounded by a magnetic coil. It is interesting to note that this plasma discharge is nearly identical to HDLT tokamak plasma conditions. These two papers set the groundwork for future investigations and applications in the area of magnetic line broadening.

An effect that is also relevant to inertial confinement fu-

*Electronic address: adams@mit.edu

sion (ICF) plasmas and pertains to the presence of a magnetic field is the translational Stark effect ($\mathbf{E}_T=\mathbf{v}\times\mathbf{B}$). The translational Stark effect was first introduced by Galushkin [9] and later in independent efforts by Isler [10] and Breton *et al.* [11]. These authors, primarily concerned with tokamak plasma, focused on the quantum mechanical problem of a hydrogen atom under the influence of both the Zeeman effect and the translational Stark effect. While their work neglected plasma broadening, it did consider correlation effects with the Doppler motion. Later, Hoe *et al.* [12] considered the translational Stark effect for ICF plasmas by adding the effect along with Doppler correlation effects to their previous work [5].

Mathys introduced the unified classical path approximation from mainstream line broadening research to magnetic line broadening [13,14], accounted for ion dynamical effects [15], and a decade later incorporated the translational Stark effect [16]. This latter work by Brillant *et al.* [16], which was initiated to study main-sequence stars with spectral types between $F0$ and $B2$ that have magnetic fields greater than 1 T, marks the first treatment of the plasma Stark effect, the translational Stark effect, and the Zeeman effect for hydrogenic emitters.

Recent research papers have reported on independent efforts to develop a magnetically broadened hydrogenic spectral line shape code [17,18]. Since this recent trend has been sparked by the magnetic confinement fusion community, it is appropriate to mention two examples, namely the development of BELINE for ALCATOR C-MOD [17] and the work of Günter-Könies for ASDEX-U [18]. These works clearly demonstrate the need for a reliable line broadening code for the magnetic confinement fusion community.

This paper uses standard line broadening theory to develop TOTALB, a computationally efficient magnetic spectral line shape model, and then applies the model to several problems of importance to the understanding of tokamak edge plasmas. Section II reviews standard line broadening by theoretical and computational methods. In order to provide a complete description of TOTALB, this section is supplemented by Appendix A, which describes the electron collision model, and Appendix B, which describes the quasistatic electric ion microfield model. Section III builds on the preceding section and systematically incorporates the magnetic field by first considering the modifications of the plasma average and then of the atomic Hamiltonian. Section IV applies TOTALB to the study of tokamak edge plasmas. Here, both direct diagnostic techniques that pertain to magnetic line shape features and radiation transport are considered. Section V provides concluding remarks and proposes future research directions.

II. GENERAL LINE SHAPE FORMALISM

In this section, the pertinent elements of the current embodiment of atomic spectral line shape calculations are discussed. No attempt at giving a complete history of the subject is made; rather the intent here is to prepare the reader for the subsequent discussion on the introduction of an external magnetic field. To supplement the topics covered in this section, the reader is encouraged to consult Griem [19], and the references therein.

A. Spectral line shape

Following Baranger [6] and Kolb and Griem [7], it is customary to begin with the quantum electrodynamical formula for the power radiated by an atom in an electric dipole transition from an initial state (i) to a final state (f):

$$P(\omega)=\frac{4\omega^4}{3c^3}\phi(\omega), \tag{1}$$

$$\phi(\omega)=\frac{1}{2\pi}\int_{-\infty}^{\infty}\Phi(t)e^{i\omega t}dt, \tag{2}$$

$$\Phi(t)=\sum_{if}\rho_i\langle\psi_i(0)|\mathbf{d}|\psi_f(0)\rangle\langle\psi_f(t)|\mathbf{d}|\psi_i(t)\rangle, \tag{3}$$

where $\phi(\omega)$ is the spectral line shape (normalized to unity $\int\phi(\omega)d\omega=1$) and $\Phi(t)$ is the time correlation function. Σ_{if} represents a sum over all final states and an average over all initial states that contribute to the line shape, ρ_i is the initial density matrix of the system, $|\psi(t)\rangle$ represents the state (in the Schrödinger picture) of the system, and $\mathbf{d}$ is the time-independent electric dipole moment of the system. The quantity $4\omega^4/3c^3$ can be added after the calculation of $\phi(\omega)$ since the frequency variation of ω^4 is small across the spectral line shape; this transfers the focus from the power radiated to the spectral line shape. To connect with dynamical theories, the initial focus is further transferred to the correlation function.

Following Fano [20], the correlation function can be simplified using general operator techniques. First, we introduce the unitary time evolution operator (U),

$$|\phi(t)\rangle=U(t,t_o)|\phi(t_o)\rangle \tag{4a}$$

$$=\exp\{-(i/\hbar)H(t-t_o)\}|\phi(t_o)\rangle, \tag{4b}$$

where H is the total Hamiltonian in Hilbert space. After inserting Eq. (4) into Eq. (3), applying the closure relation, and remembering that $\mathrm{Tr}(AB)=\mathrm{Tr}(BA)$, the correlation function becomes

$$\Phi(t)=\sum_{if}\rho_i\langle\psi_i(0)|\mathbf{d}|\psi_f(0)\rangle\langle\psi_f(0)|U^\dagger\mathbf{d}U|\psi_i(0)\rangle \tag{5a}$$

$$=\mathrm{Tr}[\mathbf{d}U\rho_i\mathbf{d}U^\dagger]. \tag{5b}$$

Next, we introduce the Liouville operator (L), which describes the time evolution of the density matrix,

$$i\hbar\frac{\partial\rho}{\partial t}=[H,\rho]\equiv L\rho. \tag{6}$$

This equation has the following solution:

$$\rho(t)=U(t)\rho(0)U^\dagger(t)=\exp\{-(i/\hbar)Lt\}\rho(0). \tag{7}$$

Notice that Eq. (7) is similar to other infinitesimal orthogonal transforms, such as the time evolution operator in Eq. (4) and the rotation operator. After inserting Eq. (7) into Eq. (5b), the general correlation function can be written as

$$\Phi(t)=\mathrm{Tr}[\mathbf{d}\exp\{-(i/\hbar)Lt\}\rho_i\mathbf{d}]. \tag{8}$$

In this form, the inverse Fourier transform in Eq. (2) has a simple solution. However, this expression is too general for tractable calculations and further approximation is necessary.

Following Fano [21], who used the Zwanzig approach [22], Eq. (8) can be simplified by separating an emitting atom from the surrounding plasma, which acts as a thermal bath. To achieve this separation, two approximations are made. First, the initial correlation between the atom (a) and plasma (p) states are neglected so that the density matrix can be written as follows:

$$\rho\rightarrow\rho^a(t)\rho^p(0)=\rho^a(t)\frac{1}{Z}\exp\left\{-\frac{H^p}{T}\right\}, \tag{9}$$

where Z is the partition function. Second, it is assumed that conditions at an earlier time do not affect the change in the density matrix at time t (Markoff approximation). These approximations affect the Liouville operator and allow the correlation function to be written in the form,

$$\Phi(t)=\mathrm{Tr}_a[\mathbf{d}\exp\{-(i/\hbar)(L^a-i\Gamma_g)t\}\rho_i^a\mathbf{d}]_{\mathrm{av}}, \tag{10}$$

where L^a is the Liouville operator pertaining to the atomic Hamiltonian, Γ_g is the general relaxation theory collisional operator, the trace is performed over all atomic states, and the average (av) is over plasma states. At this point, it is possible to introduce theoretical details of the correlation function model.

Following Griem [23], the spectral line shape calculation considers those electric dipole transitions between bound states that contribute to a well defined frequency range. The associated atomic states are grouped into an upper manifold (with states $|\alpha\rangle$) and a lower manifold (with states $|\beta\rangle$). Dipole transitions between states of the same manifold and collisional transitions between different manifolds are not considered (no quenching assumption). The plasma average is handled by separating the effects of the fast electrons and slow ions by introducing an electron collision model and a quasistatic ion microfield model into the correlation function:

$$\Phi(t)=\int P(E)\langle\langle\alpha\beta|\mathbf{d}\exp\{-(i/\hbar)(L_E^a-i\Gamma)t\}\times\rho_i^a\mathbf{d}|\alpha'\beta'\rangle\rangle dE, \tag{11}$$

where $P(E)$ is the quasistatic electric ion microfield distribution function, L_E^a is the Liouville operator pertaining to the atomic Hamiltonian for a particular ionic field (E), Γ is now the electron collision operator, and $|\alpha\beta\rangle\rangle$ represents the atomic state in Liouville (or line) space. Independent of the specific models used in the plasma average, there exists a general computational approach for solving this problem. Hence, summaries of the electron collision operator and ion microfield used in TOTALB are included in the appendices and computational details of the line shape calculation are now discussed.

Following Calisti *et al.* [4], the spectral line shape computational approach centers around solving the complex eigenvalue problem for a fixed ionic field and then averaging over possible ionic fields. Since the correlation function must be real, which requires that $\phi(-\omega)=\phi^*(\omega)$, the line shape equation can be written as

$$\phi(\omega)=\frac{1}{\pi}\mathrm{Re}\int_0^\infty\Phi(t)e^{i\omega t}dt. \tag{12}$$

After inserting Eq. (11) into Eq. (12) and performing the integration over the ion microfield last, the line shape becomes

$$\phi(\omega)=\int P(E)\frac{1}{\pi}\mathrm{Re}\int_0^\infty\langle\langle\alpha\beta|\mathbf{d}\exp\{-i/\hbar\times(L_E^a-i\Gamma)t\}\rho_i^a\mathbf{d}|\alpha'\beta'\rangle\rangle e^{i\omega t}dtdE \tag{13a}$$

$$=\sum_{j=1}^{n_E}W_j\phi(E_j,\omega), \tag{13b}$$

where the integration over E has been replaced by a sum that represents an average over discrete ionic fields with weights given by W_j. The solution of $\phi(E_j,\omega)$, the complex eigenvalue problem for fixed ionic field (E_j), is simple in the basis where $L_{E_j}^a-i\Gamma$ is diagonal.

Let $|k\rangle\rangle$ be the basis in which $L_{E_j}^a-i\Gamma$ is diagonal with complex eigenvalues $z_k(E_j)=x_k(E_j)+iy_k(E_j)$. The eigenvalues are, in general, complex since Γ is not Hermitian. In the $|k\rangle\rangle$ basis, $\phi(E_j,\omega)$ has the following inverse Fourier transform:

$$\phi(E_j,\omega)=\left\langle\left\langle\alpha\beta\left|T_{E_j}\mathbf{d}\frac{1}{\pi}\mathrm{Re}\int_0^\infty\exp\{-(i/\hbar)T_{E_j}^\dagger\times(L_E^a-i\Gamma)T_{E_j}t\}e^{i\omega t}dt\rho_i^s\mathbf{d}T_{E_j}^\dagger\right|\alpha'\beta'\right\rangle\right\rangle \tag{14a}$$

$$=\sum_k\frac{c_{1k}[\omega-x_k(E_j)]+c_{2k}y_k(E_j)}{[\omega-x_k(E_j)]^2+y_k(E_j)^2}, \tag{14b}$$

where T_{E_j} is the transformation matrix which diagonalizes $L_{E_j}^a-i\Gamma$, the sum is over eigenvalues with fixed E_j, and the coefficients c_{k1} and c_{k2} depend on $\mathbf{d}$ and T_{E_j}. Finally, the discretized spectral line shape can be written as

$$\phi(\omega)=\sum_{j=1}^{n_E}W_j\sum_k\frac{c_{1k}[\omega-x_k(E_j)]+c_{2k}y_k(E_j)}{[\omega-x_k(E_j)]^2+y_k(E_j)^2}. \tag{15}$$

In order to implement this formula, atomic structure information is needed.

B. Atomic structure

In the spectral line shape derivation, no restrictions were placed on the definition of a bound state; it can represent a hyperfine level of hydrogen or a configuration averaged level of carbon. While this approach separates the atomic structure calculations from the line shape calculations, there remains the task of constructing an optimal set of atomic data. To arrive at such a set, one uses the fact that atomic structure information only enters in the selection of states that contribute to radiation in a specific frequency range and the evaluation of the Liouville operator matrix elements. The latter is considered first.

In Liouville space, or line space, the Liouville operator matrix elements are

$$\langle\langle \alpha\beta|L_E|\alpha\beta\rangle\rangle = \hbar\omega_{\alpha\beta}, \tag{16a}$$

$$\langle\langle \alpha\beta|L_E|\alpha\beta'\rangle\rangle = \langle\beta|\mathbf{d}|\beta'\rangle E, \tag{16b}$$

$$\langle\langle \alpha\beta|L_E|\alpha'\beta\rangle\rangle = -\langle\alpha|\mathbf{d}|\alpha'\rangle E, \tag{16c}$$

where $\hbar\omega_{\alpha\beta}$ is the energy difference between states $|\alpha\rangle$ and $|\beta\rangle$, $\langle\beta|\mathbf{d}|\alpha\rangle$ is the electric dipole matrix element in the Hilbert space, and E is the ionic field strength. Thus, the atomic data information must include: (1) a label for each state; (2) quantum information ascribable to each state; and (3) electric dipole matrix elements between states.

Calculating the electric dipole matrix elements that appear in Eq. (16) requires a complete specification of the relevant quantum numbers for the states involved. Due to the spherical symmetry properties of atoms with complex atomic structure, this calculation can be simplified by using the Wigner-Eckart theorem [24] as follows:

$$\langle \gamma JM|\mathbf{d}_q^{(1)}|\gamma' J' M'\rangle = (-1)^{J-M}\begin{pmatrix} J & 1 & J' \\ -M & q & M' \end{pmatrix} \times \langle \gamma J||\mathbf{d}^{(1)}||\gamma' J'\rangle, \tag{17}$$

where tensor-operator notation has been explicitly used, the second term on the right-hand side (RHS) is a Wigner 3-j symbol and the square of the last reduced matrix element on the RHS is known as the electric dipole line strength. The electric dipole line strength includes the radial matrix element information and is independent of angular momentum coupling schemes—a detail that allows atomic structure codes based on either LS or JJ angular momentum coupling schemes to generate input for TOTALB. Now, the only atomic information necessary to calculate the electric dipole matrix elements are the $2J+1$ value of each state, which specifies the possible orientations of the 3-j symbol, and the reduced matrix elements between states.

Returning to the diagonal elements of the Liouville operator matrix elements, it is clear that energy level information is also needed to calculate the energy difference between states. The upper and lower manifolds are constructed by including only those electric dipole transitions that contribute to a given frequency range. This is done by first calculating the energy difference between states to see if the transition falls within the specified frequency range. If the transition energy is within the frequency range of interest and the electric dipole line strength is nonzero, then the associated states are included. Finally, the manifolds are supplemented by the states that contribute to Stark broadening in a manifold; again the electric dipole line strength is used.

III. INCLUSION OF AN EXTERNAL MAGNETIC FIELD

Having reviewed the general line shape formalism employed in TOTALB, it is now possible to discuss the inclusion of an external magnetic field. The magnetic field affects both the plasma average calculation and the atomic Hamiltonian. Effects of the plasma average are considered first, including both the electric ion microfield model and electron collision operator. Effects of the atomic Hamiltonian are then considered and the discussion identifies new required atomic structure information. We note that while the modification of the atomic Hamiltonian is exact, more work is needed to rigorously incorporate magnetic effects into the plasma average.

A. Plasma average modifications

The plasma average consists of two parts: the electron collision operator, which is calculated within the framework of binary collision relaxation theory, and the quasistatic electric ion microfield. An external magnetic field modifies these parts by giving the system a preferential axis. This preferential axis destroys the arbitrary orientation of the electric dipole operator and can alter the dynamical properties of the plasma.

In the absence of a magnetic field, the quasistatic ion microfield model assumes the plasma surrounding the emitting atom is spherically symmetric (see Appendix B). The electric dipole moment can be chosen to point in an arbitrary direction and the ion microfield distribution must be a function only of ionic field strength. With the introduction of an external magnetic field, and hence a preferential axis, the spherical symmetry is broken and the integration over the microfield distribution becomes anisotropic:

$$P(E)dE \rightarrow P'(E_\perp, E_\parallel)dE_\perp dE_\parallel, \tag{18}$$

where the subscripts refer to the direction of the magnetic field. This amounts to averaging over electric field directions relative to the magnetic axis. Note that, while the microfield integration has been modified, the microfield itself, which is presented in Appendix B, is assumed unchanged by the introduction of a magnetic field. This modification accounts for a majority of the increase in computational time both through the introduction of a double integration into the plasma average and tripling the number of nonzero electric dipole matrix elements that enter the complex eigenvalue problem. The following discussion considers the limitations of this model.

As an estimate to the validity of the quasistatic ion microfield model (see Appendix B), we compare a characteristic fluctuation frequency to the ion plasma frequency. In the limit that the half-width at half maximum (HWHM) of the

normalized line profile $\Delta\omega_{1/2}$ is much greater than the ion plasma frequency ω_{pi}, the quasistatic ion microfield model is valid. In the presence of an external magnetic field, the Lorentz force $q\mathbf{v}\times\mathbf{B}$ can increase the plasma frequency [25]. Thus, the condition for validity becomes less stringent and ion dynamics might be important when a magnetic field is present. A more general criterion for neglecting ion dynamics, which accounts for the asymmetry of the ion plasma frequency, is

$$\Delta\omega_{1/2} \gg \omega_{LH} \sim \omega_{pi}, \tag{19}$$

where the lower hybrid resonant frequency ω_{LH} is the ion plasma frequency perpendicular to the magnetic field. If ion dynamics is important then anisotropy should be considered further.

The literature on the importance of ion dynamics in the presence of an external magnetic is unclear [15,18]. Two authors have considered the importance of hydrogen ion dynamic effects on magnetically broadened spectral line shapes through the model microfield method (MMM). Conclusions from such an approach are not definitive since the MMM may not be applicable in the presence of a magnetic field. This topic remains unresolved and will be the study of future research.

As an estimate of the validity of the electron collision operator (see Appendix A), we examine the limit where $\Delta\omega_{1/2}$ is much less than the electron plasma frequency ω_{pe}. In the presence of a magnetic field, the Lorentz force increases the plasma frequency and increases the region of validity of the electron collision operator. The general condition for the validity of the electron collision operator can be expressed as

$$\Delta\omega_{1/2} \ll \omega_{pe} \leqslant \omega_{UH}, \tag{20}$$

where the upper hybrid resonant frequency ω_{UH} is the electron plasma frequency perpendicular to the magnetic field. While the external magnetic field strengthens the validity condition, it also introduces anisotropy.

Consideration of magnetic effects on the motion of charged particles results in a constraint on the binary collision relaxation model straight-line path (SLP) approximation. The condition for validity of the SLP approximation is that the Larmor radius must be greater than the Debye length ($r_L > \lambda_D$); or similarly the Larmor frequency must be less than the electron plasma frequency ($\omega_L = qB/2m_e < \omega_{pe}$). Explicitly writing the plasma property dependence involved in this condition places an upper limit on the magnetic field strength: $B(T) < 4.5\sqrt{n_{e14}}$, where n_{e14} is the electron density in units of 10^{14} cm^{-3}. Thus, for most HDLT edge plasma phenomenon, the SLP approximation is valid and the magnetic field does not affect the electron collision operator.

Since the approximations inherent in the electron collision operator remain valid in the presence of a magnetic field, the electron collision operator as it appears in Appendix A is unmodified in TOTALB. The neglect of magnetic field effects on the electron collision operator has been taken by other authors [16,18] and the present treatment is at no less a level of approximation.

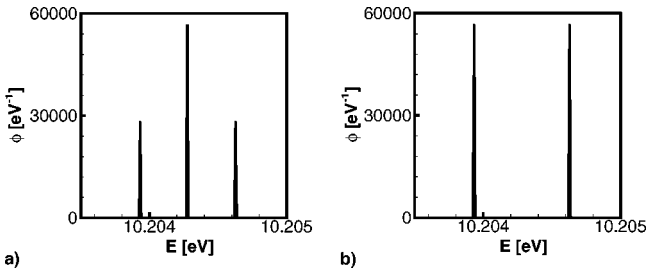

FIG. 1. Zeeman components of hydrogen Ly_α in a $B=6$ T magnetic field. The observation direction is (a) perpendicular to the magnetic axis ($\beta=\pi/2$) and (b) along the magnetic axis ($\beta=0$).

B. Atomic Hamiltonian modification

In the presence of an external magnetic field, the atomic Hamiltonian angular properties are altered—atomic energy levels are perturbed and the line shape is polarized. We use the nonrelativistic one-electron atom Hamiltonian to illustrate this modification and at the same time introduce the approximations employed. Generalization to atoms with complex structure is then accomplished through the use of Racah algebra.

The atomic Hamiltonian for a one-electron atom in a uniform external magnetic field, with vector potential $\mathbf{A}=-\frac{1}{2}\mathbf{R}\times\mathbf{B}$, is given by

$$H = \frac{1}{2m_e}[\mathbf{P} - q\mathbf{A}(\mathbf{R})]^2 + V(\mathbf{R}) \tag{21a}$$

$$= \left\{\frac{P^2}{2me} + V(\mathbf{R})\right\} - \frac{\mu_B}{\hbar}\mathbf{L}\cdot\mathbf{B} + \frac{q^2B^2}{8m_e}R_\perp^2, \tag{21b}$$

where $\mathbf{R}$ refers to the atomic electron coordinate, $\mu_B = q\hbar/2m_e$ is the Bohr magneton, $\mathbf{L}=\mathbf{R}\times\mathbf{B}$, and $R_\perp^2 = R^2 - (\mathbf{R}\cdot\mathbf{B}^2)/B^2$ is the projection of $\mathbf{R}$ onto the plane perpendicular to $\mathbf{B}$ [26]. The term proportional to $\mathbf{B}$ is called the paramagnetic term; the term proportional to B^2 is called the diamagnetic term. Assuming B is small ($B<10^3$ T), the following energy ordering applies

$$\frac{\Delta E_1}{\Delta E_0} \sim \frac{\Delta E_2}{\Delta E_1} \ll 1, \tag{22}$$

where the subscript denotes order with respect to $\mathbf{B}$. Such an energy ordering is valid for magnetic confinement fusion, where $B<10$ T, and can be written in terms of plasma properties as

$$\mu_B B = \hbar\omega_L \ll E_I = \frac{1}{2}\alpha^2 m_e c^2, \tag{23}$$

where α is the fine structure constant. Thus, the diamagnetic term is negligible compared to the paramagnetic term and will not be considered.

The change in frequency and polarization of the emitted radiation due to the paramagnetic term is collectively called the Zeeman effect. These effects are illustrated in Fig. 1. The line shapes depicted in Fig. 1 were calculated with TOTALB

using nonrelativistic atomic data and neglecting both plasma broadening and Doppler broadening. The transition energies and relative magnitudes agree with first-order perturbation theory [26].

For atoms with complex atomic structure, the paramagnetic term only affects angular properties of the atom. The general paramagnetic term can be written as

$$\mathbf{L}\cdot\mathbf{B}\rightarrow[\mathbf{J}+(g_s-1)\mathbf{S}]\cdot\mathbf{B}, \tag{24}$$

where $g_s\cong 2.00232$ is the anomalous gyromagnetic ratio for electron spin. Now the complete atomic Hamiltonian can be written as

$$H=H_0+H_S+H_Z, \tag{25}$$

where H_0 represents the full complex atomic Hamiltonian (that may include fine structure effects); H_S (Stark) and H_Z (Zeeman) are given by

$$H_S=-\mathbf{E}\cdot\mathbf{d}^{(1)}, \tag{26}$$

$$H_Z=-\mathbf{B}\cdot\boldsymbol{\mu}^{(1)}=\mu_B\mathbf{B}\cdot[\mathbf{J}+(g_s-1)\mathbf{S}]. \tag{27}$$

To evaluate the paramagnetic matrix element, let $\mathbf{B}=B\hat{z}$ and $g_s=2$. The matrix element takes the form,

$$\frac{1}{\mu_B B}\langle\gamma JM|H_Z|\gamma' J'M'\rangle=\langle\gamma JM|\mathbf{J}_0^{(1)}+\mathbf{S}_0^{(1)}|\gamma' J'M'\rangle. \tag{28}$$

In a manner similar to the electric dipole matrix element, this equation can be simplified by application of the Wigner-Eckart theorem,

$$\langle\gamma JM|\mathbf{J}_0^{(1)}+\mathbf{S}_0^{(1)}|\gamma' J'M'\rangle = (-1)^{J-M}\begin{pmatrix} J & 1 & J' \\ -M & 0 & M'\end{pmatrix}\langle\gamma J||\mathbf{J}^{(1)}+\mathbf{S}^{(1)}||\gamma' J'\rangle. \tag{29}$$

The square of the reduced matrix element on the RHS is called the magnetic dipole line strength, analogous to the electric dipole line strength. Note that the magnetic dipole line strength also includes radial matrix information and is not dependent on an angular momentum coupling scheme.

The magnetic dipole line strength is closely related to the weighted radiative transition probability (gA). More specifically

$$gA_{M1}=\xi\sum_{MM'q}\begin{pmatrix} J & 1 & J' \\ -M & q & M'\end{pmatrix}^2|\langle\gamma J||\mathbf{J}^{(1)}+\mathbf{S}^{(1)}||\gamma' J'\rangle|^2 \tag{30a}$$

$$=\xi|\langle\gamma J||\mathbf{J}^{(1)}+\mathbf{S}^{(1)}||\gamma' J'\rangle|^2, \tag{30b}$$

where ξ is a constant. Since, many atomic structure codes calculate gA in this atomic data, the reduced matrix element associated with the Zeeman effect can be easily extracted.

IV. TOKAMAK APPLICATIONS

Applications of TOTALB fall into two categories: (1) determination of local plasma properties, such as magnetic field strength, from distinct line shape features; and (2) consideration of global plasma phenomenon, such as particle and energy transport. This section considers both types of applications. In the numerical calculations that follow, we use atomic data from the relativistic complex atomic structure code HULLAC (Hebrew University Lawrence Livermore Atomic Code) [27].

A. Hydrogen resonance line

In HDLT plasmas, the resonance line of hydrogen (Ly_α) has a significant optical depth ($\tau\sim\chi L>1$, where χ is the line radiation absorption coefficient and L is a length characterizing the extent of the plasma region). Since details of the spectral line shape will affect the plasma opacity, it is interesting to quantify magnetic field effects on τ.

To begin, the line radiation absorption coefficient for a plasma in local thermodynamic equilibrium (LTE) [28] is

$$\chi(\nu)=n_i B_{ij}\frac{h\nu_{ij}}{4\pi}\phi_{ij}(\nu)\left[1-\exp\left\{-\frac{h\nu_{ij}}{T}\right\}\right] \sim n_i\left\{\frac{e^2}{4\pi\varepsilon_0}\frac{\pi}{mc}\phi_{ij}(\nu)\right\}f_{ij}, \tag{31a}$$

$$\chi_0\sim n_{i14}\left\{\frac{0.011}{\Delta E_{\mathrm{eV}}}\right\}f_{ij}(\mathrm{cm}^{-1}), \tag{31b}$$

where i (j) refers to the lower (upper) level of a bound-bound transition, B is the Einstein B coefficient, $h\nu_{ij}$ is the line center energy, ϕ is the line profile, T is the thermodynamic temperature, f is the line absorption oscillator strength, χ_0 is the line center absorption coefficient, n_{i14} is the neutral level density in units of $10^{14}\,\mathrm{cm}^{-3}$, and ΔE is the full-width at half maximum (FWHM) of the line shape in units of eV. In Eqs. (31a) and (31b), the terms in curly brackets represent an effective cross section for photon absorption. The latter equation demonstrates the inverse proportionality between ΔE and χ_0. As a line becomes broader, the oscillator strength is distributed over a greater frequency range. With χ_0 given by Eq. (31b), the optical depth can be estimated with a suitable choice of L.

The effect of an external magnetic field on opacity can be quantified by using TOTALB. As an example, Fig. 2 depicts a typical hydrogen Ly_α line shape for an HDLT plasma ($n_e=10^{15}\,\mathrm{cm}^{-3}$ and $T_e=1$ eV), with ($B=6$ T, solid line) and without ($B=0$ T, dashed line) an external magnetic field. As the magnetic field increases from $B=0$ T to 6 T, the FWHM increases from $\Delta E=0.0009$ eV to 0.0011 eV. Setting $L=1$ cm and choosing a ground state density of $n_1=10^{14}\,\mathrm{cm}^{-3}$ yields values without (with) magnetic effects: absorption coefficient of $5.1\,\mathrm{cm}^{-1}$ ($4.2\,\mathrm{cm}^{-1}$); effective photon mean free path of 0.20 cm (0.24 cm); and optical depth of 5.1 (4.2). Thus, magnetic line broadening reduces the optical depth by $\approx 18\%$.

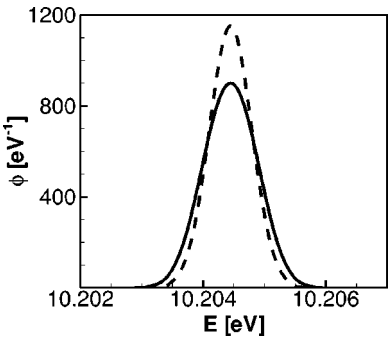

FIG. 2. Hydrogen Ly_α line shape with an external magnetic field ($B=6$ T, solid line) and without ($B=0$ T, dashed line). Plasma conditions are: $n_e=10^{15}$ cm^{-3} and $T_e=1$ eV. The direction of observation is perpendicular to the magnetic axis ($\beta=\pi/2$).

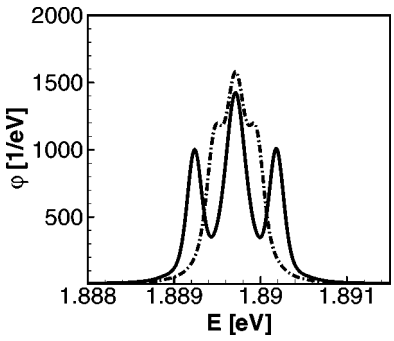

FIG. 3. Magnetic field strength variation from $B=4$ T (dash-dot line) to $B=8$ T (solid line). Plasma conditions are: $n_e=10^{15}$ cm^{-3} and $T_e=1$ eV. The angle of observation is perpendicular to the magnetic axis ($\beta=\pi/2$).

While magnetic line broadening significantly affects the spectral line shape, the signature feature of the Zeeman effect, namely the Lorentz triplet present in Fig. 1(a) does not appear. At $T=1$ eV, the Doppler width is approximately $\Delta E_D \sim 8\times10^{-4}$ eV, which is comparable to the Zeeman splitting $\Delta E_Z \simeq 2\mu_B B \sim 7\times10^{-4}$ eV and thus masks the Lorentz triplet.

B. Magnetic field diagnostic

Equation (25) has three terms on the RHS: H_0 pertains to the energy of a state; H_S leads to the Stark effect and is proportional to the plasma density as well as the principal quantum number (which scales approximately as n^2) [24]; and H_Z leads to the Zeeman effect and is proportional to **B**. Thus, the shift and intensity of a spectral line shape component are dependent on the relative contributions of both the Stark effect and the Zeeman effect. Furthermore, the intensity of a component will vary with the angle of observation relative to the magnetic axis due to the polarization properties of the Zeeman effect. From these line shape properties, if the Zeeman effect dominates the Stark effect then both the magnetic field strength and the angle of the magnetic field relative to the direction of observation can be accurately determined using TOTALB.

For HDLT plasmas in the ALCATOR C-MOD tokamak, H_α is a prime magnetic field diagnostic candidate. High-resolution, H_α measurements are made routinely in ALCATOR C-MOD [29] and the data clearly exhibit the Zeeman effect signature [3]. While these measurements were intended to study the hydrogen to deuterium ratio and plasma fluctuations, they are ideally suited for magnetic field diagnostic purposes.

To demonstrate the magnetic field diagnostic procedures, we first determine the magnetic field strength. Figure 3 shows the sensitivity of H_α to changes in the magnetic field strength for conditions typical of an HDLT plasma; notice how the energy of a σ component moves further from the central π component as the magnetic field strength increases. Given the electron density and electron temperature (and ion temperature if it is different), the magnetic field strength is determined by numerically matching the energy difference between the central π component and a σ component. This is not the same as inferring the magnetic field from the first-order Zeeman effect alone ($\Delta E_{1/2}=\mu_B B$), since this would be valid only in the absence of plasma broadening. To quantify the error made by neglecting plasma broadening, the magnetic field strength calculated using only the first-order Zeeman formula with $\Delta E_{1/2}$ taken from the $B=8$ T curve in Fig. 3 would be 8.21 T. In this case, the result is an overestimate of the magnetic field strength by 0.21 T, which would lead to a significant difference in the inferred emission region in a tokamak.

At this point, it is interesting to quantify the validity conditions of Sec. III A. In order to neglect ion dynamics, we require $\Delta\omega_{1/2} \gg \omega_{LH} \sim \omega_{pi}$. From Fig. 3 and various definitions of the HWHM $\Delta\omega_{1/2} \sim 2-9\times10^{11}$ s^{-1}, using $B=6$ T, we have $\omega_{LH} \sim 2\times10^{10}$ s^{-1} and $\omega_{pi} \sim 4\times10^{10}$ s^{-1}. Thus, $\Delta\omega_{1/2} \gg \omega_{pi} > \omega_{LH}$ and the quasistatic electric ion microfield model is at least as valid as in the absence of a magnetic field. To ensure the validity of our binary collision relaxation model, we require $\Delta\omega_{1/2} \ll \omega_{pe} \lesssim \omega_{UH}$ and $B(T) < 4.5\sqrt{n_{e14}}$. Using $B=6$ T, we have $\omega_{UH} \sim 2.1\times10^{12}$ s^{-1} and $\omega_{pe} \sim 1.8\times10^{12}$ s^{-1}, thus the first inequality, is valid; inserting the electron density into the second inequality, we find the following upper limit on the magnetic field $B(T) < 14(T)$ and can safely say the second inequality is valid.

Figure 4 shows the line shape from an angle of observation along the magnetic axis, with the same plasma conditions as in Fig. 3, and reveals a better candidate for determining magnetic field strength. The absence of the central π component allows the diagnostic to be applied to lower mag-

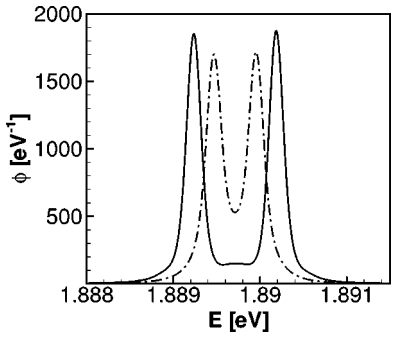

FIG. 4. Same plasma conditions as in Fig. 3 but now the angle of observation is along the magnetic axis ($\beta=0$).

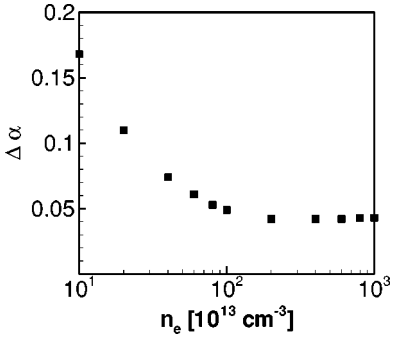

FIG. 5. A plot of the H_β HWHM including the $n_e^{2/3}$ scaling ($\Delta\alpha=\Delta\lambda_{1/2}/n_e^{2/3}$) as a function of electron density. The curve asymptotes when the linear Stark effect dominates other broadening mechanisms. Plasma properties are: $B=6$ T, $T_e=2$ eV, and $\beta=\pi/2$.

netic field tokamaks at a fixed experimental resolution. Figures 3 and 4 also illustrate the variation in intensity, but not shift, of the line profile components with an angle of observation relative to the magnetic axis (β). For an arbitrary β, the spectral line shape intensity is given by

$$\phi(\omega,\beta)=\cos^2(\beta)\,\phi_\parallel(\omega)+\sin^2(\beta)\,\phi_\perp(\omega). \qquad (32)$$

This property can be used to determine β by numerically matching the relative intensity of the π component to a σ component.

C. Electron density diagnostic

In plasmas without an external magnetic field, the spectral line width is commonly used to determine plasma densities. For instance, Griem recommends H_β as an excellent candidate for determining the electron density in plasmas where $n_e>10^{14}$ cm^{-3} [19]. In this density regime, the linear Stark effect dominates over other broadening mechanisms and the FWHM scales as $n_e^{2/3}$. Below an electron density of 10^{14} cm^{-3}, fine structure effects begin to enter and the dominant FWHM dependence makes a transition from the linear Stark effect to the quadratic ion impact [30].

In plasmas with an external magnetic field, the Stark effect competes with the Zeeman effect. Günter-Könies [18] investigated the feasibility of H_β as a density diagnostic for low magnetic field tokamaks ($B\sim 2$ T) and found it to be useful, provided $n_e>2\times10^{14}$ cm^{-3}. We comment that this result is sensitive to the plasma average and their valid density range is decreased when ion dynamics is neglected. Figure 5, which was calculated for conditions typical of ALCATOR C-MOD ($B=6$ T) and uses a more appropriate plasma average, indicates that H_β is not useful as an electron density diagnostic unless $n_e>2\times10^{15}$ cm^{-3} or the $n_e^{2/3}$ scaling is abandoned for a numerical fit. Future interpretations of H_β data can rely on TOTALB to predict electron density, however current interpretations that neglect magnetic field effects should rely on higher-n Balmer lines to take advantage of the n^2 Stark scaling, e.g., $H_{8\rightarrow2}$.

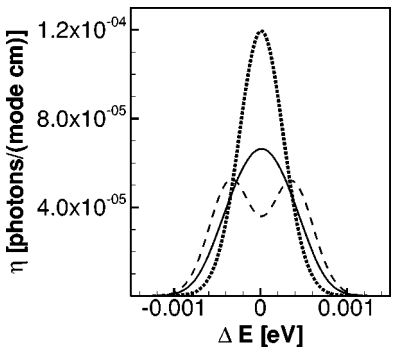

FIG. 6. Ly_α emissivity at the center of the plasma slab. The solid curve ($\beta=\pi/2$) and the dashed curve ($\beta=0$) are magnetically broadened lines shapes; the dotted line is without magnetic field effects included.

D. Finite plasma slab

HDLT tokamak edge plasmas strongly interact with hydrogen line radiation. Thus, in HDLT plasmas, the details of spectral line shapes will determine the spatial and frequency variation of opacity, which in turn influences the spatial variation in level populations and ultimately the transport of energy. Through full integration of TOTALB into a coupled nonlocal thermodynamic equilibrium (NLTE) atomic kinetics and radiation transfer code CRETIN [31], the effects of magnetically broadened line shapes can be quantified.

We consider a one-dimensional plasma slab in the x-y plane with a thickness of $L=1$ cm and plasma properties: $\mathbf{B}=6\hat{x}$ T, $T_e=1.0$ eV, $n_e=10^{15}$ cm^{-3}, and $n_1=10^{14}$ cm^{-3} (ground state neutral hydrogen density). Figure 6 demonstrates the Ly_α emissivity variation with angle relative to the magnetic axis. Figure 7 shows the variation in optical depth of the plasma slab with (solid line) and without (dotted line) magnetic field effects. Figure 8 plots the spectral radiation intensity escaping the plasma slab with (solid line) and without (dotted line) magnetic field effects. The intensity integrated over energy increased by $\approx$10%—this difference increases with optical depth. Magnetic field effects will not directly affect the integrated intensity of optically thin lines since all the emitted photons in an optically thin line escape and their distribution relative to line center is irrelevant. However, optically thick lines can affect the excited state

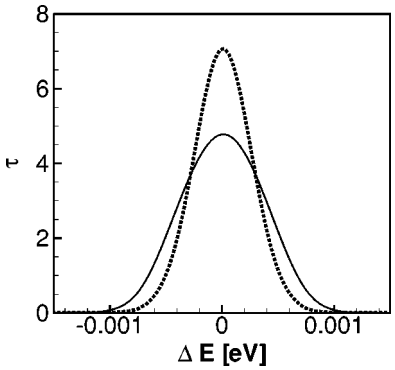

FIG. 7. Ly_α optical depth of the finite plasma slab with (solid line) and without (dotted line) magnetic field effects.

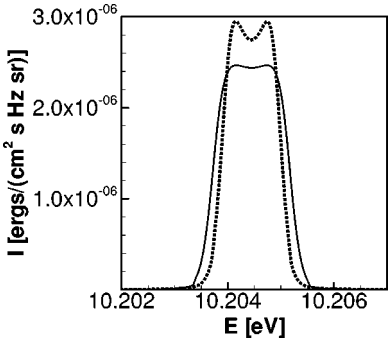

FIG. 8. Ly_α spectral radiation intensity escaping the finite plasma slab with (solid line) and without (dotted line) magnetic field effects.

population distribution, leading to changes in emission from optically thick lines, as well as ionization, recombination, and energy loss rates [32].

V. DISCUSSION

The effects of an external magnetic field have been added to the spectral line broadening model TOTAL [4] and the goal of producing an atomic line shape model that includes magnetic effects and can be included into larger transport codes has been reached; the resulting model is TOTALB. However, while the atomic Hamiltonian modification is complete and the conditions for the modification of the plasma average have been obtained, future work on incorporating magnetic effects into the plasma average is needed for a more robust model.

Since the region of validity of the quasistatic ion microfield is restricted by anisotropic ion dynamics, future research is needed to determine the role of $P(E_\parallel, E_\perp)$, the conditional probability, in regimes where ion dynamics may become important. Since the SLP approximation is out of the region of validity, research is needed to look at anisotropic electron collision dynamics. Also, development of a test to evaluate the detailed role of electron impact models is warranted, especially since this may lead to further reduction of computational cost.

While these areas of future research limit the general applicability of TOTALB, there still exist numerous applications to tokamak edge plasmas, as well as other systems in plasma physics, condensed matter physics, and astrophysics. For tokamak applications, simulation of atomic spectral lines, such as carbon and boron, is now possible and can potentially lead to numerous new direct diagnostic techniques. More interesting for the design and optimization of next generation fusion experiments and burning plasmas is the possibility of quantifying radiation effects on edge plasma transport.

ACKNOWLEDGMENTS

MLA would like to thank A.S. Wan (LLNL) and J.P. Freidberg (MIT) for their valuable contributions. This work was performed under the auspices of the U.S. Department of Energy by the University of California, Lawrence Livermore National Laboratory, through Contract No. W-7405-Eng-48. Partial support was also provided by the U.S. Department of Energy HEDS Grant No. DE-FG03-98DP00213 to Howard University.

APPENDIX A: ELECTRON COLLISION OPERATOR

The electron collision operator represents the effect of the electron field on the radiator and is usually calculated within the framework of a binary collision relaxation theory. The main difference from the standard impact approximation is to take into account the change of the electron collision operator with respect to the increase of the frequency separation from the line center [for example, $\Gamma(\Delta\omega) \neq \Gamma(0)$].

The electron collision operator (Γ), traditionally obtained by invoking the impact theory, corrected for a frequency dependent impact parameter cutoff (the Lewis cutoff [33]) is modified to give the following expression of the frequency dependent collisional operator [34,35]:

$$\Gamma(\Delta\omega) = \frac{1}{3\pi}\sqrt{\frac{2m_e}{\pi T}} n_e \left(\frac{h}{m_e}\right)^2 \mathbf{d}\cdot\mathbf{d}\left(C_n + \frac{1}{2}\int_{y(\Delta\omega)}^{\infty} e^{-x}\frac{dx}{x}\right), \tag{A1}$$

where $\mathbf{d}$ is the electric dipole operator, m_e is the perturber mass, C_n is a strong collision term that depends on the principal quantum number n, and $y(\Delta\omega)$ is given by

$$y(\Delta\omega) \sim \left(\frac{\hbar n^2}{2}\right)^2 \frac{\omega_{pe}^2 + \Delta\omega^2}{E_I T}, \tag{A2}$$

where ω_{pe} is the electron plasma frequency and E_I is the ionization energy of hydrogen. Note that in these appendices, cgs units are in use with the exception of temperature in energy units.

The final line shape has the following form:

$$\phi(\Delta\omega) \propto \begin{cases} \dfrac{\Gamma}{\Delta\omega^2 + \Gamma^2} & 0 \leqslant \Delta\omega \leqslant \omega_{WF}, \\ (\Delta\omega)^{-5/2} & \Delta\omega \geqslant \omega_{WF}, \end{cases} \tag{A3}$$

where ω_{WF} is the Weisskopf frequency, and for $\Delta\omega \geqslant \omega_{WF}$ the electrons are supposed to be static and the corresponding line shape is well described by the Holtsmark theory [36].

Here, it is important to point out that this frequency dependent collision operator is used in post processing and, consequently, no extra computational time is needed. The calculated transitions are dressed, not with a Lorentzian as usual, but with the appropriate frequency dependent function.

APPENDIX B: ELECTRIC-ION MICROFIELD

The method of generating the electric ion microfield for use in the line shape formalism is discussed by Iglesias *et al.* [37], and we include a description here for completeness. The electric microfield distribution gives the probability density of finding an electric field $\boldsymbol{\varepsilon}$ at an ion of charge $Z_0 e$ located at the origin due to an ionic mixture where ions of

species σ carry charge $Z_\sigma e$. Here, e is the magnitude of the elementary charge and the Z's are positive and zero for a neutral radiator. As usual, the electron screening is described by the Debye-Hückel formula [38]. This is justified only for weak electron-electron and electron-ion coupling and nondegenerate electrons. The system is therefore described by classical equilibrium statistical mechanics with a radiator plus N ions at temperature T_i.

In the thermodynamic limit, where $N\rightarrow\infty$ in such a way that the ion number density n_i is constant, the system is isotropic and setting $\varepsilon=|\boldsymbol{\varepsilon}|$ yields the following distribution of the electric field magnitude [39,40]:

$$P(\varepsilon)=4\pi\varepsilon^2\langle\delta(\boldsymbol{\varepsilon}-\mathbf{E})\rangle \tag{B1a}$$

$$=\frac{2\varepsilon}{\pi}\int_0^\infty \lambda\,\sin(\lambda\varepsilon)T(\lambda)d\lambda, \tag{B1b}$$

with characteristic function given by

$$T(\lambda)=\langle\exp\{i\boldsymbol{\lambda}\cdot\mathbf{E}\}\rangle, \tag{B2}$$

where the brackets $\langle\ldots\rangle$ denote an equilibrium ensemble average over the ions.

The potential energy is given by a sum of pairwise additive electron-screened ion-ion interactions,

$$V=\sum_{j=1}^{N} u_{0\sigma_j}(r_{\sigma_j})+\sum_{1\leqslant i<j\leqslant N} u_{\sigma_i\sigma_j}(|\mathbf{r}_{\sigma_j}-\mathbf{r}_{\sigma_i}|), \tag{B3}$$

where the first term describes the interaction of the radiator with the N perturbing ions and the second, the interaction among the N perturbers. The assumed interaction has the form,

$$u_{ij}=Z_iZ_je^2\frac{e^{-k_er}}{r}, \tag{B4}$$

where $k_e^2=4\pi n_e e^2/T_e$ is the inverse Debye length, with n_e and T_e as the electron number density and temperature, respectively. The total electric field is given by the sum of electron-screened single-ion contributions,

$$\mathbf{E}=\sum_{j=1}^{N}\boldsymbol{\varepsilon}_{\sigma_j}(\mathbf{r}) \tag{B5a}$$

$$=-\frac{1}{Z_0e}\sum_{j=1}^{N}\boldsymbol{\nabla}_{\sigma_j}u_{0\sigma_j}(r_{\sigma_j}) \tag{B5b}$$

$$=\sum_{j=1}^{N}Z_{\sigma_j}e\hat{r}_{\sigma_j}f(r_{\sigma_j}), \tag{B5c}$$

where $\hat{r}$ is the unit vector in the direction of $\mathbf{r}$ and

$$f(r)=\frac{(1+k_er)}{r^2}e^{-k_er}. \tag{B6}$$

An important quantity is the second moment of the distribution [41]

$$\langle\mathbf{E}\cdot\mathbf{E}\rangle=\frac{4\pi n_iT_i}{Z_0}k_e^2\sum_\sigma Z_\sigma c_\sigma\int_0^\infty re^{-k_er}g_\sigma(r)dr, \tag{B7}$$

where $g_\sigma(r)$ and c_σ denote the radial distribution (RDF) around the radiator and relative abundance of species σ, respectively.

The APEX approximation [41,42] can be derived from a renormalized cluster expansion, which maximizes the independent-particle contribution relative to the Baranger-Mozer series [43]. The APEX method has been described previously and only the main results are quoted. The initial step is to introduce effective single particles with adjustable parameters $\{\alpha_\sigma\}$,

$$\varepsilon_\sigma^*(r)=Z_\sigma e\hat{r}\frac{1+\alpha_\sigma r}{r^2}e^{-\alpha_\sigma r} \tag{B8a}$$

$$=Z_\sigma e\hat{r}F_\sigma(r), \tag{B8b}$$

an equation which defines $F_\sigma(r)$. Then the characteristic function for the effective independent particles becomes

$$T_{\mathrm{APEX}}(\lambda)=\exp\left\{4\pi n_i\sum_\sigma c_\sigma\int_0^\infty r^2g_\sigma(r)\frac{f(r)}{F_\sigma(r)}\times(j_0[\lambda Z_\sigma eF_\sigma(r)]-1)dr\right\} \tag{B9}$$

making the APEX result the first term in a renormalized cluster expansion [43]. The adjustable parameters $\{\alpha_\sigma\}$ are chosen to satisfy the second moment rule [41],

$$\int_0^\infty r^2g_\sigma(r)f(r)F_\sigma(r)dr=\frac{T_i}{Z_0Z_\sigma e^2}k_e^2\int_0^\infty re^{-k_er}g_\sigma(r)dr. \tag{B10}$$

Hence, the RDF's provide a scheme for evaluating the microfield distribution.

Spectral line broadening calculations require large field values of the microfield distribution. While large fields are not encountered in HDLT plasma hydrogenic spectral line shapes, for a complete description of the microfield, we briefly comment on our treatment. The large field limit is given by the nearest neighbor (NN) result; that is, for large fields the distribution is dominated by a single particle at a short distance from the radiator [44]. Therefore,

$$P(\varepsilon)|_{\varepsilon\rightarrow\infty}\rightarrow P_{NN}(\varepsilon)=4\pi\varepsilon^2n_i\sum_\sigma c_\sigma\times\int g_{\sigma,NN}(r)\delta[\boldsymbol{\varepsilon}-\boldsymbol{\varepsilon}_\sigma(\mathbf{r})]d\mathbf{r}, \tag{B11}$$

where $P_{NN}(\varepsilon)$ and $g_{\sigma,NN}(r)$ are the microfield distribution and RDF for the nearest neighbor to the radiator, respectively. Unfortunately, the evaluation of $g_{\sigma,NN}(r)$ is difficult

[45], except within the framework of simplifying approximations. For example, the case of independent ions yields [46,47]

$$g_{\sigma,NN}(r)\simeq\exp\left\{-\frac{u_{0\sigma}(r)}{T_i}\right\}\exp\left\{4\pi n_i\sum_{\sigma'}\ c_{\sigma'}\times\int_0^{r_\sigma}y^2\exp\left[-\frac{u_{0\sigma'}(y)}{T_i}\right]dy\right\}. \tag{B12}$$

The first exponential factor gives the probability of finding an ion of species σ at a distance r; the second exponential factor is the probability that no other ion is within the radius r. To account for perturber correlations, it is common practice to replace $\exp\{-u(r)/T_i\}$ by $g(r)$. Thus,

$$P_{NN}(\varepsilon)\simeq 4\pi n_i\sum_{\sigma}\ c_\sigma r_\sigma^2 g_\sigma(r_\sigma)\exp\left\{4\pi n_i\sum_{\sigma'}\ c_{\sigma'}\times\int_0^{r_\sigma}y^2 g_{\sigma'}(r)dy\right\}\left|\frac{d\varepsilon_\sigma(r)}{dr}\right|^{-1}_{r=r_\sigma}, \tag{B13}$$

where $\varepsilon=Z_\sigma f(r_\sigma)$ defines the nearest neighbor radii $\{r_\sigma\}$.

Finally, we note that the microfield distribution involves the sine transform in Eq. (B1b). Unfortunately, this integral becomes numerically unstable for large fields. The problem is partially alleviated by using the asymptotic nearest neighbor microfield distribution result, Eq. (B13). However, under certain conditions, the numerical difficulties begin before the asymptotic limit is reached.

To evaluate the sine transform, the new version of the APEX program used a method developed to compute the integrals of oscillatory functions. The integral in Eq. (B1b) is evaluated over half cycles of the sine function. The Levine t transform [48,49] then provides a computationally efficient method for evaluating the resulting alternating series.

As indicated above, the RDF's are a central ingredient in the APEX formulation of the microfield. For Coulomb and screened Coulomb systems, the hypernetted chain (HNC) integral equation approach provides reasonably accurate results [50]. While HNC calculations are not needed for HDLT plasmas, for a complete description of the microfield, we briefly comment on our treatment. The HNC approximation consists of dropping the so-called bridge diagrams in the RDF expression, that is,

$$g_{ij}(r)=\exp\left\{-\frac{u_{ij}(r)}{T_i}+h_{ij}(r)-c_{ij}(r)+B_{ij}(r)\right\}, \tag{B14}$$

where the HNC approximation assumes $B(r)=0$. Here, $h(r)$ is the total correlation function,

$$h_{ij}=g_{ij}(r)-1 \tag{B15}$$

and $c(r)$ the direct correlation function defined by the Ornstein-Zernike equation,

$$h_{\sigma_i\sigma_j}(r_{ij})=c_{\sigma_i\sigma_j}(r_{ij})+n_i\sum_{\sigma_k}\ c_{\sigma_k}\int_0^\infty c_{\sigma_i\sigma_k}(r_{ik})h_{\sigma_k\sigma_j}(r_{kj})dr_k. \tag{B16}$$

The method of solution is to set $B(r)=0$ and iterate between Eqs. (B14), (B15), and (B16). The initialization is achieved by first estimating $c(r)$ using the analytic fits of Pingolet-Held [51]. This provides an improved starting point; it reduces the number of iterations, compared to other simple choices such as the Debye-Hückle result. More importantly, it provides robust solutions for the cases of interest here; spectroscopically observable bound-bound transitions.

After initialization, the iteration proceeds toward convergence, which is assumed when the root mean square of the deviations of two successive iterations of $c(r)$ is small. However, the convergence can be extremely slow. The acceleration technique due to Ng [52] has proven very successful. It is found empirically that the Ng acceleration is most robust when employed only after every tenth iteration. This detail, of course, depends on the nature of the potential.

[1] C.S. Pitcher and P.C. Stangeby, Plasma Phys. Controlled Fusion **39**, 779 (1997).
[2] R. Stambouch *et al.*, Nucl. Fusion **39**, 2391 (1999).
[3] M.L. Adams, H.A. Scott, R.W. Lee, J.L. Terry, E.S. Marmar, B. Lipschultz, A.Yu. Pigarov, and J.P. Freidberg, J. Quant. Spectrosc. Radiat. Transf. **71**, 115 (2001).
[4] A. Calisti, F. Khelfaoui, R. Stamm, B. Talin, and R.W. Lee, Phys. Rev. A **42**, 5433 (1990).
[5] N. Hoe, H.W. Drawin, and L. Herman, J. Quant. Spectrosc. Radiat. Transf. **7**, 429 (1967).
[6] M. Baranger, Phys. Rev. **111**, 494 (1958).
[7] A.C. Kolb and H.R. Griem, Phys. Rev. **111**, 514 (1958).
[8] H.W. Drawin, H. Henning, L. Herman, and N. Hoe, J. Quant. Spectrosc. Radiat. Transf. **9**, 317 (1969).
[9] Yu.L. Galushkin, Astron. Zh. **47**, 375 (1970).
[10] R.C. Isler, Phys. Rev. A **14**, 1015 (1976).
[11] C. Breton, C. DeMichelis, M. Finkenthal, and M. Mattioli, J. Phys. B **13**, 1703 (1980).
[12] N. Hoe, J. Grumberg, M. Caby, E. Leboucher, and G. Coulaud, Phys. Rev. A **24**, 438 (1981).
[13] G. Mathys, Astron. Astrophys. **125**, 13 (1983).
[14] G. Mathys, Astron. Astrophys. **139**, 196 (1984).
[15] G. Mathys, Astron. Astrophys. **141**, 248 (1984).
[16] S. Brillant, G. Mathys, and C. Stehlé, Astron. Astrophys. **339**, 286 (1998).
[17] L.G. D'yanchkov, V.G. Novikov, A.F. Nikiforov, A.Yu. Pigarov, and V.S. Vorob'ev, Report No. MIT PSFC/RR-99-9, 1999 (unpublished).
[18] S. Günter and A. Könies, J. Quant. Spectrosc. Radiat. Transf. **62**, 425 (1999).
[19] H.R. Griem, *Principles of Plasma Spectroscopy* (Cambridge University Press, New York, 1997).

[20] U. Fano, Rev. Mod. Phys. **29**, 74 (1957).
[21] U. Fano, Phys. Rev. **131**, 259 (1963).
[22] R. Zwanzig, J. Chem. Phys. **33**, 1338 (1960).
[23] H.R. Griem, *Spectral Line Broadening by Plasmas* (Academic Press, New York, 1979).
[24] R.D. Cowan, *The Theory of Atomic Structure and Spectra* (University of California Press, Berkeley, CA, 1981).
[25] F.F. Chen, *Introduction to Plasma Physics and Controlled Fusion*, 2nd ed. (Plenum Press, New York, 1984).
[26] C. Cohen-Tannoudji, B. Diu, and F. Laloë, *Quantum Mechanics* (Wiley, New York, 1977).
[27] A. Bar-Shalom, M. Klapisch, and J. Oreg, J. Quant. Spectrosc. Radiat. Transf. **71**, 169 (2001).
[28] D. Mihalas, *Stellar Atmospheres*, 2nd ed. (Freeman, New York, 1978).
[29] E.S. Marmar, S.J. Zweben, S. Fulghum, and P.S. Rostler, Rev. Sci. Instrum. **70**, 1 (1999).
[30] D.E. Kelleher, W.L. Wiese, V. Helbig, R.L. Greene, and D.H. Oza, Phys. Scr., T **T47**, 75 (1993).
[31] H.A. Scott, J. Quant. Spectrosc. Radiat. Transf. **71**, 689 (2001).
[32] M.L. Adams and H.A. Scott, Contrib. Plasma Phys. **42**, 395 (2002).
[33] M. Lewis, Phys. Rev. **121**, 501 (1961).
[34] H.R. Griem, Astrophys. J. **136**, 422 (1962).
[35] H.R. Griem, Astrophys. J. **147**, 1092 (1967).
[36] J. Holtsmark, Ann. Phys. (Leipzig) **7**, 578 (1919).
[37] C.A. Iglesias, F.J. Rogers, R. Shepherd, A. Bar-Shalom, M.S. Murillo, D.P. Kilcrease, A. Calisti, and R.W. Lee, J. Quant. Spectrosc. Radiat. Transf. **65**, 303 (2000).
[38] R.J. Tighe and C.F. Hooper, Phys. Rev. A **15**, 1773 (1977).
[39] M. Baranger and B. Mozer, Phys. Rev. **115**, 521 (1959).
[40] B. Mozer and M. Baranger, Phys. Rev. **118**, 626 (1960).
[41] C.A. Iglesias, H.E. DeWitt, J.L. Lebowitz, D. MacGowan, and W.B. Hubbard, Phys. Rev. A **31**, 1698 (1985).
[42] C.A. Iglesias, J.L. Lebowitz, and D. MacGowan, Phys. Rev. A **28**, 1667 (1983).
[43] J.W. Dufty, D.B. Boercker, and C.A. Iglesias, Phys. Rev. A **31**, 1681 (1985).
[44] J.W. Dufty and L. Zogaib, Phys. Rev. A **44**, 2612 (1991).
[45] C.A. Iglesias, C.F. Hooper, and H.E. DeWitt, Phys. Rev. A **28**, 361 (1983).
[46] M. Lewis and H. Margenau, Phys. Rev. **109**, 842 (1958).
[47] M. Lewis and H. Margenau, Rev. Mod. Phys. **31**, 569 (1959).
[48] D. Levine, J. Comput. Math. **B3**, 371 (197).
[49] A. Bar-Shalom, M. Klapisch, and J. Oreg, Comput. Phys. Commun. **93**, 21 (1996).
[50] F.J. Rogers, J. Chem. Phys. **73**, 6272 (1980).
[51] B. Held and R. Pingolet, J. Phys. **47**, 437 (1986).
[52] K. Ng, J. Chem. Phys. **61**, 2680 (1974).